Journal of Alloys and Compounds 505 (2010) 598–603

Contents lists available at ScienceDirect

Journal of Alloys and Compounds

journal homepage: www.elsevier.com/locate/jallcom

Effects of silicon content on the microstructure and corrosion behavior of Fe–Cr–C hardfacing alloys

G. Azimi [a], M. Shamanian [b,*]

[a] Educational Workshop Center, Isfahan University of Technology (IUT), Isfahan 8415683111, Iran
[b] Department of Materials Engineering, Isfahan University of Technology (IUT), Isfahan 8415683111, Iran

ARTICLE INFO

Article history:
Received 29 October 2009
Received in revised form 14 June 2010
Accepted 16 June 2010
Available online 25 June 2010

Keywords:
Fe–Cr–C
Coating
Corrosion
Microstructure

ABSTRACT

Three Fe-based alloys, namely 55Fe39Cr6C, 49Fe39Cr6C6Si, and 45Fe39Cr6C10Si (wt.%), were fabricated on AISI St52 using a tungsten-inert gas (TIG) heat source. Microstructure, microhardness, and electrochemical corrosion behavior of the TIG clad composite coatings were investigated. It was found that as-deposited coatings consisted of higher volume fractions of carbides (Cr_7C_3). Potentiodynamic polarization studies in the 3.5 wt.% NaCl solution showed that the corrosion resistance of the substrate was remarkably improved by TIG surface coating (TSC) with 55Fe39Cr6C and 49Fe39Cr6C6Si, while 45Fe39Cr6C10Si had a lower effect on this same property. The formation of silicides (Fe_3Si) in the clad with 45Fe39Cr6C10Si was taken as the reason for the reduced corrosion resistance observed as compared to those of the other clads.

1. Introduction

The superior abrasive and erosive wear resistance of Fe–Cr–C alloys results from great amounts of hard carbides with excellent corrosion resistance. The abrasion wear resistance is reported to be dependent upon not only type, morphology, amount, and distribution pattern of the carbides precipitated from the melt, but also the type of matrix structure [1]. In general, the microstructure observations of Fe–Cr–C alloys have shown that these types of materials contain hypoeutectic, eutectic and hypereutectic structures [2–4]. The hypoeutectic microstructures consist of primary dendrites of austenite (γ) phase and eutectic colonies ($\gamma + M_7C_3$). The hypereutectic microstructures include the primary M_7C_3 carbides and eutectic colonies ($\gamma + M_7C_3$).

Much attention has been focused on the wear behavior of Fe–Cr–C alloys and several models have also been developed for the microstructure–property relationship of these alloys [5–11]. However, the slurries are often corrosive in the oil sand production.

Erosion–corrosion causes a serious problem for the oil sands industry where handling and processing of essentially silica-based solids results in extremely severe corrosion and wear conditions [12]. The Cr_7C_3 is well known for its excellent combination of high hardness and wear resistance as well as good corrosion and oxidation resistance, so, it has been widely used as the reinforcing phase in the composite coatings [13–16]. However, the information on the performance of these alloys in the corrosive environments is yet limited in the open literature [17,18]. Therefore, the utilization of this carbide to improve the corrosion and wear properties would be interesting.

On the other hand, addition of silicon to metals and alloys, including steels, generally increases their resistance against corrosion, oxidation, and erosion [19]. Despite this, silicon addition changes the mechanical properties of the alloys and increases their production costs [20]. However, silicon coatings can instead be used to overcome this limitation as they improve the corrosion resistance of steels without changing the mechanical properties of the bulk materials [21–23]. A wide range of coating techniques have been used for obtaining Si coatings that include chemical vapor deposition (CVD), physical vapor deposition (PVD), pack cementation, and ion implantation [24]. Coatings with filler metals or powders are mostly made by welding, thermal spraying, or allied welding processes [25]. In recent years, a number of studies conducted on the gas tungsten arc welding (GTAW) process to modify the properties of steel surface [26–30]. In this study, the surface of the carbon steel was intrinsically alloyed with preplaced 55Fe39Cr6C, 49Fe39Cr6C6Si, and 45Fe39Cr6C10Si powders using a tungsten arc heat source under a shield of pure argon gas. The goal of this study was to investigate the effect of Si content on the microstructures and corrosion resistance of Fe–Cr–C claddings.

2. Materials and methods

The base metals (110 mm × 40 mm × 10 mm) for the TIG cladding were prepared from St52 steel plates with the chemical composition as specified in Table 1. Before cladding, the specimens were ground and cleaned with acetone. Mixtures of Fe, Cr,

* Corresponding author. Tel.: +98 311 3915737; fax: +98 311 3915737.
E-mail address: shamanian@cc.iut.ac.ir (M. Shamanian).

0925-8388/$ – see front matter © 2010 Elsevier B.V. All rights reserved.
doi:10.1016/j.jallcom.2010.06.084

Table 1
Chemical compositions of the specimen (St52 steel) and powders for surface alloying (wt.%).

Chemical component	Fe	C	Si	Mn	Cr
St52 steel	98.29	0.216	0.218	0.951	–
55Fe39Cr6C powder	55	6	–	–	39
49Fe39Cr6C6Si powder	49	6	6	–	39
45Fe39Cr6C10Si powder	45	6	10	–	39

Table 2
GTAW operating parameters.

Electrode	W-2% thorium
Diameter	2.4 mm
Electrode polarity	DCEN
Welding current (A)	120
Welding speed (m/s)	1.3×10^{-3}
Argon, flow rate (L/min)	8

Si, and graphite powders were used as the cladding materials. The compositions of the powders used for surface alloying are also given in Table 1.

In order to form alloy filler (105 mm × 30 mm × 1.5 mm), a constant high pressure was exerted to the powders. The alloy filler was then placed on the base metal. Table 2 presents the different cladding conditions used in this research.

After surface alloying, samples were cut from the alloyed specimens for microstructural examination and microhardness measurement. Preparation for metallographic examination consisted of grinding on SiC wheels followed by polishing. The coatings were etched by 2% nital, while the base metal was etched by chloride ferric alcohol. Conventional characterization techniques such as optical microscopy, scanning electron microscopy (SEM), energy dispersive spectrograph (EDS), and X-ray diffraction were employed for studying the microstructure and elemental analysis of the alloyed zone. The microhardness values with a 100 g load were taken across the alloyed zone.

The corrosion behavior of the TIG clad and as-received samples were studied using potentiodynamic polarization (Tafel analysis) in a 3.56 wt.% NaCl solution from −250 to +250 mV (SCE) at a scan rate of 1 mV/s using standard calomel as the reference electrode and platinum as the counter electrode [31]. Corrosion current density (i_{corr}) was determined from the intersection of the respective anodic and cathodic Tafel slopes.

3. Results and discussion

3.1. Microstructure characterization

Fig. 1 shows the cross-sectional optical micrograph of the clad layers formed by TIG with 55Fe39Cr6C (Fig. 1a), 49Fe39Cr6C6Si (Fig. 1b), and 49Fe39Cr6C10Si (Fig. 1c) powder mixtures. It is evident that the clad layers are adherent, crack/defect free and consist of two zones comprising a columnar morphology followed by a dendritic structure.

Clad layer thicknesses varied over 2–2.2 mm under the TSC (TIG Surface Cladding) described above (Table 1). The difference in clad thickness deposit due to the cladding process was manual. Variation of the etching contrast suggests that partial melting of the substrate and intermixing could not be avoided during TSC. A thin white layer was observed on the interface, which indicates good metallurgical bonding between the deposited coating and the substrate.

At the bonding zone, an extremely high rate of heat transfer occurred between the molten pool and the substrate and a large melt was obtained under cooling leading to a very high rate of solidification. The solid–liquid interface would grow in a flat form giving rise to the formation of a bright flat grain in the coating as shown in Fig. 1.

Fig. 2 shows the SEM images of the clad matrix with 55Fe39Cr6C powder mixtures. The microstructure consists of primary austenite and a eutectic phase of austenite and carbides. Using an X-ray diffractometer (Fig. 3) and EDS analysis (Fig. 4), the carbides were identified to be Cr_7C_3, which is in agreement with findings reported in the literature [32–39]. The onset of solidification coincided with

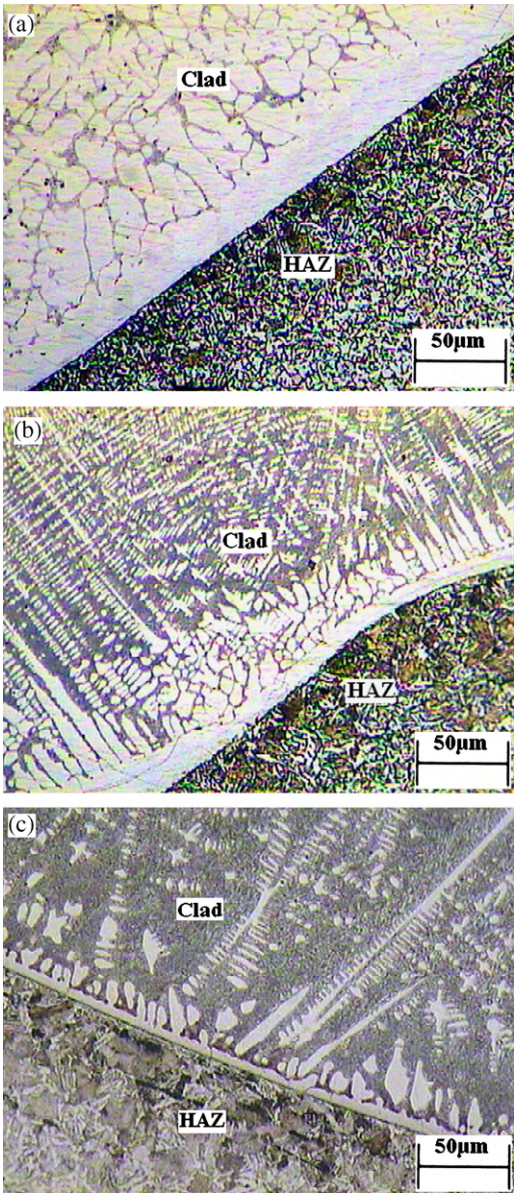

Fig. 1. Cross-sectional optical micrographs of the clad layers formed by GTAW with (a) 55Fe39Cr6C, (b) 49Fe39Cr6C6Si, and (c) 45Fe39Cr6C10Si powder mixtures.

the formation of primary austenite while the binary eutectic phase of austenite and Cr_7C_3 transformed from the remaining melt. At room temperature and in the as-solidified condition, both types of austenite (primary and eutectic) were present as retained austenite [32–39]. The details of microstructural investigation of the samples coated by FeCrC powders are given in Ref. [40].

The typical microstructure of the TSC with 49Fe39Cr6C6Si powder is shown in Fig. 5. The composite coating consists of a primary phase and a small amount of fine interdendritic eutectic. The primary phase presents a fine dendritic shape. Based on the results obtained from both XRD (Fig. 6) and EDS analyses, the primary phase is identified as austenite and the fine interdendritic eutectic is confirmed to consist of Fe_7C_3, Cr_7C_3 carbides and the iron-base solid solution γ. It may also be concluded that the iron-base solid solution is saturated with the Si element. In area A (Fe–9.2%Cr–2.4%Si), there is the deposit of dendritic γ-Fe, which is a non-equilibrium phase with an extended solid solution of the alloying elements of Cr and Si, the latter only in small amounts. In area B (Fe–33%Cr–1.4%Si), the eutectic of γ-(Fe,Cr,Si) and carbide is generated. Accompanying the

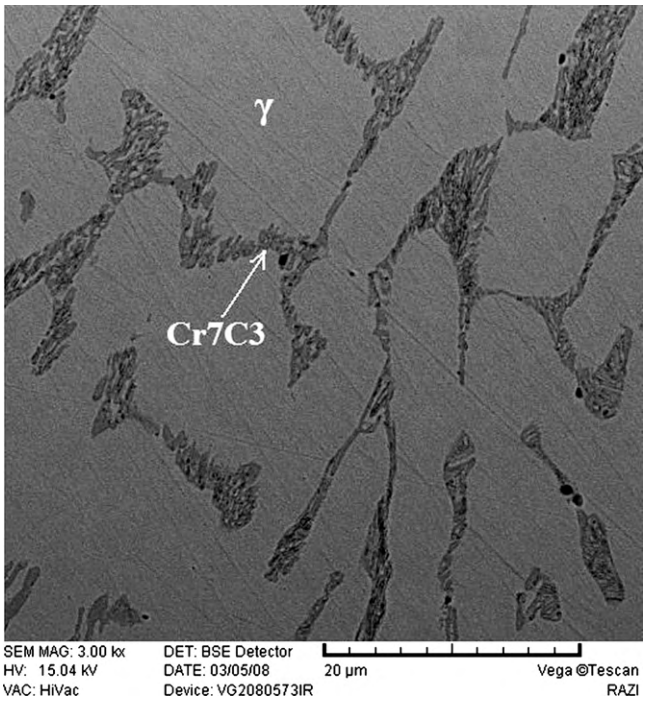

Fig. 2. SEM micrograph of the alloyed zone of the specimen alloyed with 55Fe39Cr6C powder.

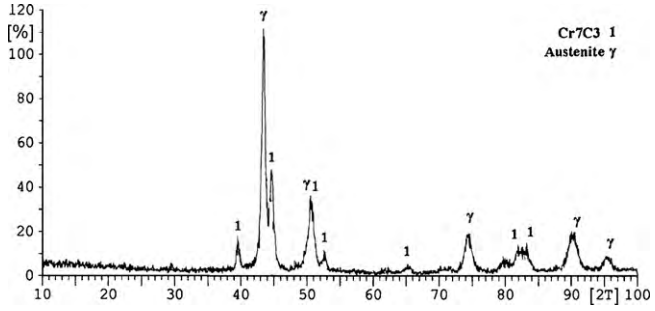

Fig. 3. X-ray diffraction spectrum obtained from the alloyed zone with the 55Fe39Cr6C powder.

formation of the primary dendritic γ-(Fe,Cr,Si), the residual melt is enriched in carbon and chromium and the eutectic of γ/$(Cr,Fe)_7C_3$ is subsequently formed when the concentration in the residual melt reaches a certain level.

Cr_7C_3 carbides are usually covered with another phase, which makes it almost impossible to identify these carbides through the optical microscope [41]. In this study, only Cr_7C_3 could be

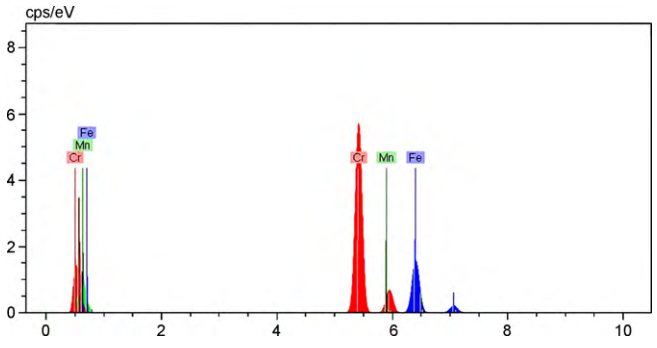

Fig. 4. EDS spectra of the alloyed zone in the specimen alloyed with the 55Fe39Cr6C powder.

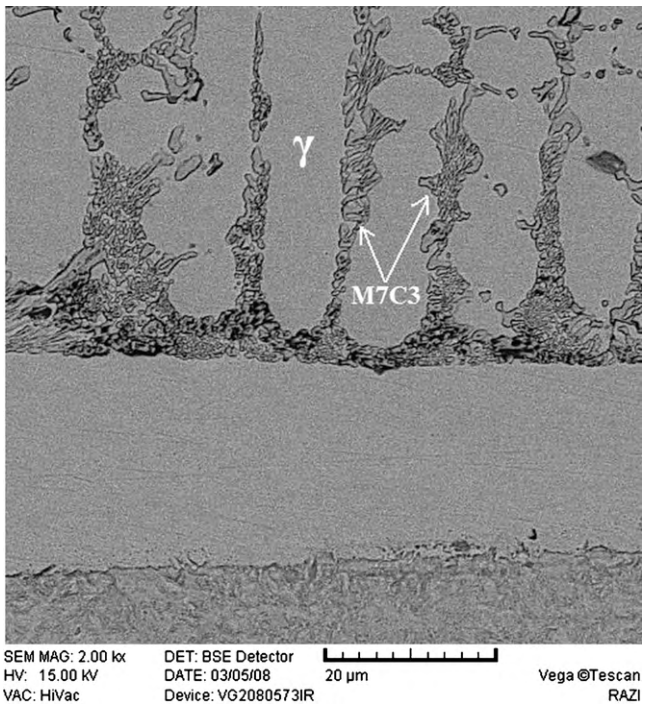

Fig. 5. SEM micrograph of the alloyed zone of the specimen alloyed with the 49Fe39Cr6C6Si powder.

detected using a back-scattered electron image (BEI), as shown in Fig. 5.

Fig. 6 shows the X-ray diffraction pattern of TIG clad St52 steel with the 49Fe39Cr6C6Si and 45Fe39Cr6C10Si powders. It can be seen that the composite coating consists of γ-Fe, Cr_7C_3 and Fe_7C_3 phases. In the XRD profile, no silicate phase is detected. However, in the case where the powder blend for cladding contains 6 wt.% Si, Si is detected in EDS analysis of the clad layer. The absence of separate peaks for silicides suggests that Si in the powder blend could have been dissolved in the γ-Fe solid solution [42].

Si is known to have a very low solubility in carbides [43] (and specifically also M_7C_3 [43]). In the case of the surface coating with 49Fe39Cr6C6Si, Si in the powder blend could have been dissolved in the γ-Fe solid solution. Si is found to influence significantly the morphology of M_7C_3 carbides. A further effect of Si is to reduce Cr concentration of the austenite. This is advantageous because Cr is better used in the formation of M_7C_3 carbides [44].

The typical microstructure of TSC with the 45Fe39Cr6C10Si powder is shown in Fig. 7. Results of X-ray diffractometer (XRD),

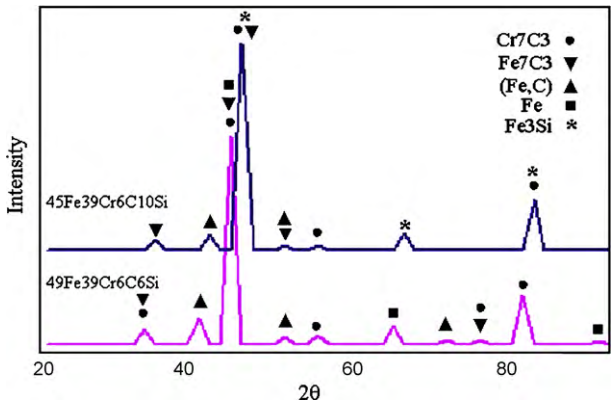

Fig. 6. X-ray diffraction spectrum obtained from the surfaces alloyed with 49Fe39Cr6C6Si and 45Fe39Cr6C10Si powders.

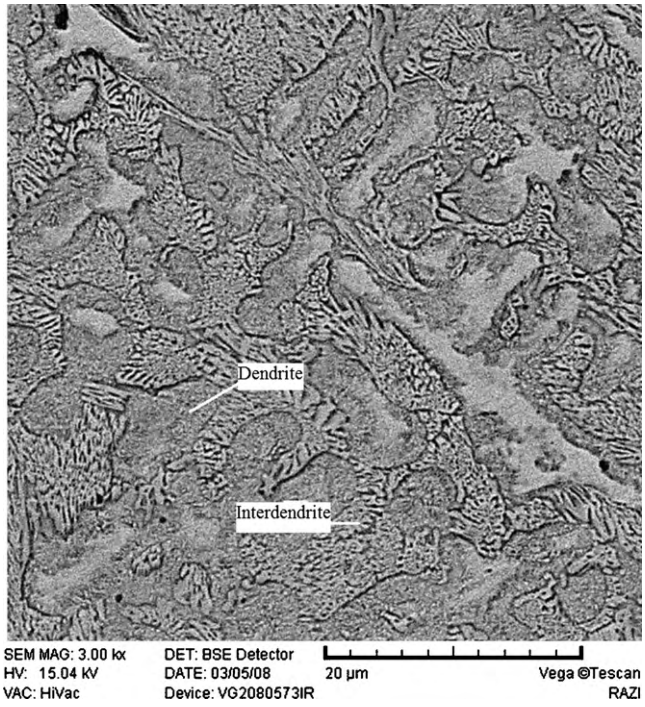

Fig. 7. SEM micrograph of the alloyed zone of the specimen alloyed with the 45Fe39Cr6C10Si powder.

shown in Fig. 6, indicate that the main phases are austenite γ-Fe(Cr,Si) and the compounds Fe_7C_3, Cr_7C_3, and Fe_3Si. The dark area in Fig. 7 represents the deposit of denderitic γ-Fe, which is a non-equilibrium phase with an extended solid solution of the alloying elements Cr and Si, the latter only in small amounts. The bright area in which the eutectic of γ-Fe, carbide, and Fe_3Si were generated, the main elements are Cr, Fe, Si, and C. Accompanying the formation of the primary dendritic γ-Fe, the residual liquid is enriched in carbon, Silicon, and chromium while the eutectic of γ-Fe + alloy carbide and Fe_3Si is subsequently formed when the concentration in the residual liquid reaches a certain level. The carbide and the Fe_3Si are uniformly distributed in the austenite γ-Fe(Cr,Si), as shown in Fig. 7.

The EDS microanalysis shown in Fig. 8 reveals that the coating is principally composed of Si, Cr, and Fe. The atomic percentages obtained from the EDS analysis presented in Fig. 8 and in agreement with phase diagram [45] suggest that the possible phase formed on the surface of steel is Fe_3Si. This was confirmed by the XRD analysis showing the characteristic peaks corresponding to Fe_3Si.

However, phases rich in Si, such as FeSi, are formed at higher temperatures or for longer times and this leads to the formation of a coating that spalls easily [28]. But powders used for this coating

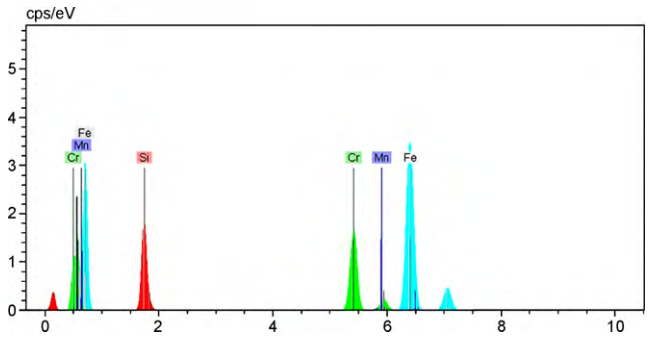

Fig. 8. EDS spectra of the specimen alloyed with the 45Fe39Cr6C10Si powder.

consisted of a small amount of Si (10 wt.%) while the cooling rate in the welding was high so that the chances for Si-rich silicates to form (such as FeSi and Fe_5Si_3) were very low. This was confirmed by XRD analysis showing the characteristic peaks corresponding to Fe_3Si.

3.2. Corrosion

Fig. 9 shows the Tafels plots derived from the potentiodynamic polarization studies of (1) as-received and TIG surface clad AISI St52 steel with (2) 55Fe39Cr6C, (3) 49Fe39Cr6C6Si, and (4) 45Fe39Cr6C10Si, respectively. The corrosion current (i_{corr}) and corrosion potential (E_{corr}) values for the respective samples are obtained from the intersection of cathodic and anodic Tafel plots. Accordingly, the corrosion rate is determined using the following relation:

$$\text{Corrosion rate (mpy)} = (CWi_{corr})/\rho$$

where C = conversion factor, W = equivalent weight of test specimen (g), ρ = density of the material (mg/m^3), and i_{corr} = current density (μA/cm^2). Polarization resistance, which is an indirect measure of corrosion resistance, is subsequently calculated using the following relation [31]:

$$\text{Polarization resistance; } \frac{dE}{di} = \frac{\beta_a\beta_c}{2.3i_{corr}(\beta_a+\beta_c)}$$

where β_a and β_c are the slopes of tangents drawn on the respective anodic and cathodic polarization plots. Table 3 summarizes the corrosion rate and polarization resistance calculated from the Tafels plot achieved by potentiodynamic polarization testing in a 3.56 wt.% NaCl solution. A detailed analysis of the corrosion data reveals that TSC St52 steel with 55Fe39Cr6C, 49Fe39Cr6C6Si, and 45Fe39Cr6C10Si reduces the corrosion rate significantly compared to that of the substrate. Furthermore, TIG clad AISI St52 steel with 49Fe39Cr6C6Si shifted the corrosion potential to the nobler side. The superior corrosion resistance property of TIG clad AISI St52 steel with 49Fe39Cr6C6Si as compared to that of the substrate and other clad compositions is also evident from the highest value of polarization resistance calculated from the corrosion parameters (β_a, β_c, i_{corr}) derived from the Tafels analysis (Table 3). It appears that corrosion performance was influenced by the phase composition of these clads.

3.2.1. Potentiodynamic polarization curves

Generally, the corrosion reaction of iron-base alloys in a solution containing dissolved oxygen with near-neutral pH may be written as follows [46]:

$$\text{Anodicreaction : } Fe \rightarrow Fe^{2+} + 2e^- \quad (1)$$

$$\text{Cathodicreaction : } (1/2)O_2 + H_2O + 2e^- \rightarrow 2OH^- \quad (2)$$

$$\text{Overallreaction : } 2Fe + 2H_2O + O_2 \rightarrow 2Fe^{2+} + 4OH^- \rightarrow 2Fe(OH)_2\downarrow \quad (3)$$

Dynamic polarization diagrams in 3.5% NaCl aqueous solution for the Fe–Cr–C cladding with various Si contents are shown in Fig. 9. It was evident that the corrosion potential of the cladding with 49Fe39Cr6C6Si was higher than that of 55Fe39Cr6C and 45Fe39Cr6C10Si. This indicates that 6%Si content led to nobler corrosion potential for Fe–Cr–C claddings.

The corrosion potential of $(Cr,Fe)_7C_3$ carbides in Fe–Cr–C cladding is believed to be nobler than that of austenite. The chromium content of $(Cr,Fe)_7C_3$ is higher than that of austenite. Therefore, the $(Cr,Fe)_7C_3$ is nobler than austenite. As a result, the

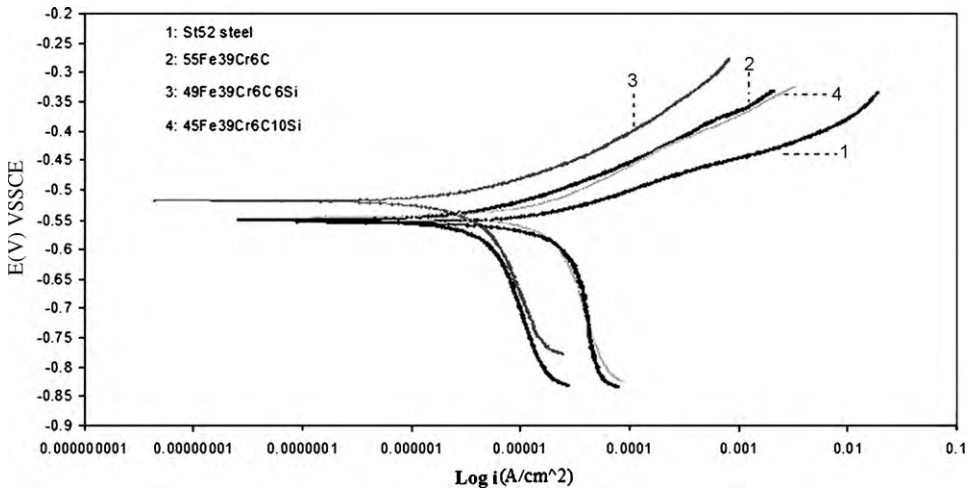

Fig. 9. Variation in current density with potential in the potentiodynamic polarization study in the 3.56 wt.% NaCl solution for (1) as-received and TIG surface clad AISI St52 steel and that with (2) 55Fe39Cr6C, (3) 49Fe39Cr6C6Si, and (4) 45Fe39Cr6C10Si. The calculated corrosion rates are summarized in Table 3.

Table 3
Corrosion properties of clad layers and substrate.

Clad composition/substrate (wt.%)	E_{corr} (V)	i_{corr} (μA)	Corrosion rate (mpy)	Polarization resistance (Ω cm^2)
Substrate	−0.556	25	11.44	9.5×10^2
54Fe40Cr6C	−0.520	5	2.9	6.42×10^3
49Fe39Cr6C6Si	−0.552	5	1.89	6×10^4
45Fe39Cr6C10Si	−0.546	20	7.61	1.71×10^3

more $(Cr,Fe)_7C_3$ carbides can change the corrosion potential of cladding to nobler direction [47,48].

On the other hand, Si is known to have a very low solubility in carbides [43] (specifically in M_7C_3 [43]). In the case of the surface coating with 49Fe39Cr6C6Si, Si in the powder blend can be dissolved in the γ-Fe solid solution. Si can significantly affect the morphology of M_7C_3 carbides. Another effect of Si is to reduce Cr concentration of the austenite. This effect is advantageous because Cr is better used in the formation of M_7C_3 carbides [44]. Therefore, the corrosion resistance of cladding was enhanced by the great amounts of $(Cr,Fe)_7C_3$ carbides.

However, Si content decreased in the austenite in the case of surface coating with 45Fe39Cr6C10Si due to the formation of Fe_3Si. Cr concentration of the austenite increased and thus amounts of $(Cr,Fe)_7C_3$ carbides decreased. Consequently, the corrosion resistance decreased with decreasing of the amount of $(Cr,Fe)_7C_3$ carbides.

These results indicates that the $(Cr,Fe)_7C_3$ carbides exhibit nobler corrosion potential than the austenite [47,48]. In these conditions, the austenitic matrix can be attacked and corroded due to galvanic corrosion.

Because the $(Cr,Fe)_7C_3$ carbides is more corrosion resistant, the corrosion potential of $(Cr,Fe)_7C_3$ carbides was higher than that of austenitic matrix. The $(Cr,Fe)_7C_3$ carbides became nobler and the austenitic matrix became more active. Therefore $(Cr,Fe)_7C_3$ carbides and austenitic matrix can form a galvanic couple. However, the area fraction of each phase is also important for the corrosion behavior. If the area of corroded austenitic matrix is less, the corrosion resistance will be improved at the same time. As long as the resistant $(Cr,Fe)_7C_3$ carbides increased, the corrosion resistance of claddings enhanced. Finally, the corrosion resistance was proportioned to the amount of resistant phase.

The corrosion current of the surface coating with 49Fe39Cr6C6Si (5 μA) was reduced to about 1/5 of the substrate (25 μA), also it could be seen that the values of polarization resistance increased from 9.5×10^2 to 6×10^4 Ω cm^2 (Table 3). The corrosion resistance of the surface coating with 49Fe39Cr6C6Si was about 63 times higher than that of the substrate. Consequently, the higher polarization resistance, nobler corrosion potential and lower corrosion current indicates better corrosion resistance of cladding. As a result, the best corrosion resistance was obtained in the cladding with 49Fe39Cr6C6Si, but the worst one occurred in the cladding with 45Fe39Cr6C10Si. The corrosion resistance of the cladding with 49Fe39Cr6C6Si was approximately 35 times higher than that of with 45Fe39Cr6C10Si.

4. Conclusions

In this study, Fe–Cr–C and Fe–Cr–Si–C coatings were fabricated on plain carbon steel using the TIG cladding technique. The following conclusions may be drawn from our findings:

- Coatings produced by TIG cladding with premixed powders are free from pores or cracks and show good metallurgical bonding with the substrate. Typical coating thickness is about 2–2.5 mm.
- The corrosion resistance of the substrate was remarkably improved by TIG surface coatings (TSC) with 55Fe39Cr6C and 49Fe39Cr6C6Si, but the effect of 45Fe39Cr6C10Si had a lower effect in improving corrosion resistance.
- The presence of 6%Si in the coating increases corrosion resistance.

References

[1] Y. Matsubara, N. Sasaguri, K. Shimizu, S.K. Yu, Wear 250 (2001) 502.
[2] L. Lu, H. Soda, A. McLean, Mater. Sci. Eng. A 347 (2003) 214.
[3] C. Fan, M.C. Chen, C.M. Chang, W. Wu, Surf. Coat. Technol. 201 (2006) 908.
[4] C.W. Kuo, C. Fan, S.H. Wu, W. Wu, Mater. Trans. 48 (2007) 2324.
[5] C.M. Chang, C.M. Lin, C.C. Hsieh, J.H. Chen, W. Wu, J. Alloys Compd. 487 (2009) 83.
[6] S. Buytoz, M.M. Yildirim, H. Eren, Mater. Lett. 59 (2006) 607.
[7] Y.F. Liu, Z.Y. Xia, J.M. Han, G.L. Zhang, S.Z. Yang, Surf. Coat. Technol. 201 (2006) 863.
[8] C.M. Lin, C.M. Chang, J.H. Chen, C.C. Hsieh, W. Wu, Metall. Mater. Trans. A 40A (2009) 1031.

[9] C.M. Chang, C.M. Lin, C.C. Hsieh, J.H. Chen, C.M. Fan, W. Wu, Mater. Chem. Phys. 117 (2009) 257.
[10] A. Neville, F. Reza, S. Chiovelli, T. Revega, Metall. Mater. Trans. A 37A (2006) 2339.
[11] C.M. Chang, Y.C. Chen, W. Wu, Tribol. Int. 43 (2010) 929.
[12] H.M. Clark, R.J. Llewellyn, Wear 250 (2001) 32.
[13] A.F. Zhang, J.D. Xing, L. Fang, J.Y. Su, Wear 257 (2004) 198.
[14] P.Q. La, Q.J. Xue, W.M. Liu, Wear 249 (2001) 93.
[15] C.T. Liu, J.O. Steigler, F.H. Sam Fores, Metal Handbook, 10th ed., The Materials Information Society, USA, 1990, p. 913.
[16] S. Frangini, A. Masci, A.D. Bartolomeo, Surf. Coat. Technol. 149 (2002) 279.
[17] R.B. Davis, Microstructural Relationship to Flow Accelerated Corrosion, Code and Standard for Quality Engineering, ASME, Minneapolis, MN, 1994, p. 3.
[18] Z. Yue, P. Zhou, J. Shi, Wear of Materials, ASME, New York, 1987, p. 763.
[19] J.T.K. Clark, A.I. Foster, M.L. Sims, M.A.M. Swidzinski, D. Young, Chemical Vapour Deposition, Eindhoven, Netherlands, 1983.
[20] A. Sanjurjo, S. Hettiarachchi, K.H. Lau, P. Cox, B. Wood, Surf. Coat. Technol. 54/55 (1992) 224.
[21] S.S. Ionayoshi, S. Tsukahara, A. Kinbara, Vacuum 53 (1999) 281.
[22] J. Perez Mariano, J. Elvira, F. Plana, C. Colominas, Surf. Coat. Technol. 200 (18/19) (2006) 5606.
[23] A. Sanjurjo, B. Wood, K. Lau, G. Krishnan, Scr. Metall. Mater. 31 (8) (1994) 1019.
[24] J. Porcayo-Calderón, E. Brito Figueroa, J.G. Gonzaléz-Rodriguez, Mater. Lett. 38 (1999) 45.
[25] J.R. Davis, ASM Handbook, Welding, Brazing and Soldering, vol. 6, ASM International, USA, 1993, pp. 787–799.
[26] S.W. Wang, Y.C. Lin, Y.Y. Tsai, J. Mater. Proc. Technol. 140 (2003) 682.
[27] M. Eroğlu, N. Özdemir, Surf. Coat. Technol. 154 (2002) 209–217.
[28] S. Buytoz, M. Ulutan, Surf. Coat. Technol. 200 (2006) 3698.
[29] S. Buytoz, Surf. Coat. Technol. 200 (2006) 3734.
[30] X. Wang, L. Cheng, M. Zhang, Z. Zou, Surf. Coat. Technol. 203 (2009) 976–980.
[31] M.G. Fontana (Ed.), Corrosion Engineering, McGraw-Hill, New York, 1987, p. 71.
[32] J.A. Pero-Sanz, J. Asensio, Mater. Charact. 43 (1999) 33–39.
[33] M. Izciler, H. Celik, J. Mater. Process. Technol. 105 (2000) 234–245.
[34] M.M. Arikan, H. Cimenoglu, E.S. Kayali, Wear 247 (2001) 231–235.
[35] ASM Handbook, Heat Treating, vol. 4, ASM International, 1993.
[36] C.P. Tabrett, I.R. Sare, J. Mater. Sci. (2000) 2069–2077.
[37] H. Berns, A. Fischer, Mater. Charact. 39 (1997) 499–525.
[38] O.N. Dongan, A.J. Hnwk, G.I.I. Laird, Metall. Mater. Trans. A 28A (1997) 1315–1328.
[39] A. Kagawa, S. Kawashima, Y. Ohta, Mater. Trans. A 28A (1997) 1171–1177.
[40] O. Yilmaz, M. Ozenbas, S. Buytoz, Mater. Sci. Technol. 18–10 (2002) 1209.
[41] C. Fan, W. Wu, C.-M. Chang, M.-C. Chen, Surf. Coat. Technol. (2006) 908–912.
[42] Manna, et al., Surf. Coat. Technol. 201 (2006) 434–440.
[43] L.E. Svensson, B. Gretoft, B. Ulander, H.K.D.H. Bhadeshia, J. Mater. Sci. 21 (1986) 1015.
[44] S. Atamert, H.K.D.H. Bhadeshia, Proceedings of Heat Treatment “87”, Institute of Metals, London, 1988, pp. 39–43.
[45] A. Il'Inskii, S. Slyusarenko, O. Slukhovskii, I. Kaban, W. Hoyer, Non-Cryst. Solids 306 (2002) 90–98.
[46] B. Lu, J. Luo, S. Chiovelli, Metall. Mater. Trans. A 37 (2006) 3029.
[47] C.M. Chang, C.C. Hsieh, C.M. Lin, J.H. Chen, C.M. Fan, W. Wu, Mater. Chem. Phys. (2010), doi:10.1016/j.matchemphys.2010.04.003.
[48] L. Junbo, Wuh. Univer. J. Natu. Sci. 12 (2007) 1109–1112.